374794-2-T

# RADIATION AND SCATTERING FROM CAVITY BACKED SLOT ANTENNAS USING THE FINITE ELEMENT-ADAPTIVE INTEGRAL METHOD

**S.S. Bindiganavale, K. Filipovic and J.L. Volakis**

**Rockwell International**
**Science Center**
**1049 Camino Dos Rios**
**P.O. Box 1085**
**Thousand Oaks, CA 91360**

January 1998

374794-2-T = RL-2542

# Radiation and Scattering from Cavity-Backed Slot Antennas Using the Finite Element-Adaptive Integral Equation Method

Radiation Laboratory
Department of Electrical Engineering and Computer Science
The University of Michigan
Ann Arbor, MI 48109-2122

**Abstract**

This paper considers the implementation of the Adaptive Integral Method (AIM) on the Boundary Integral (BI) subsystem to reduce storage requirement and solution time associated with iterative solutions of Finite Element - Boundary Integral (FE-BI) systems. Analysis of cavity-backed antennas possessing fine details such as slot arrays, spirals and log-periodics, with the FE-BI technique leads to large boundary integral systems which limit the size of such simulations. In this paper, we show the benefits of AIM when applied to compute the boundary integral matrix-vector products. Significant reduction in storage requirements and CPU time are achieved with very little loss of accuracy in computing impedances and radiation patterns of cavity-backed antennas.

# 1 Introduction

Fast integral equation methods were introduced in computational electromagnetics in the early 1990s and have been shown effective in accelerating the computation of matrix-vector products in iterative solvers. The Adaptive Integral Method (AIM) [1] and the Fast Multipole Method (FMM) [2] belong to this class of fast integral solution techniques. Both AIM and FMM reduce the solution time and memory requirement of the moment method (MM) solutions and their initial applications focussed on electromagnetic scattering from large conducting bodies. More recently, they have also been used successfully in hybrid methods such as the FE-BI method [3],[4], [5],[6] to evaluate the scattering from composite structures. FMM achieves its CPU reduction by grouping the far-zone unknowns and interacting their weighted contributions. In the case of AIM, the CPU reduction is achieved by mapping the original MM discretization onto a rectangular grid and exploiting the Toeplitz property of the Green's function on this grid. That is, the Fast Fourier Transform (FFT) is invoked to compute the matrix-vector products in the iterative solver. For an arbitrary three dimensional body, a three dimensional FFT is required and as can be understood, this calculation is very time consuming. For planar scatterers and radiators the dimensionality of the FFT is reduced by one, thereby significantly accelerating the solution.

In this paper, we consider the implementation of AIM in connection with to a finite element-boundary integral solutions radiation and scattering by cavity-backed antennas. The modeling of such antennas has been discussed extensively [7], [8],[9],[10] and it is known that considerable computational challenges are present when the surface aperture is associated with antennas possessing fine details as is the case with thin slot and thin printed antennas.

For such geometries, the number of boundary integral unknowns balloons due to the high rate of discretization needed for accurate simulation. In these situation, AIM is very attractive for reducing memory and CPU requirements. Although certain approximations are introduced when mapping the irregular grid to a rectangular uniform grid, the input impedance can still be computed at sufficient accuracy.

# 2 FE-BI formulation for cavity-backed antennas

Consider a cavity-backed antenna recessed in a ground plane as depicted in Figure 1. This class of configurations have been modeled using the finite element [8],[10],[11] very successfully. The most rigorous of the implementations is to employ the finite element method to model the interior volume below the cavity and the boundary integral for truncating the finite element mesh on the antenna/cavity aperture [8],[10].

To develop the necessary linear equations, a standard approach is to begin with the weighted residual equation

$$\begin{aligned} \iiint_V \{(\nabla \times \mathbf{T}) \cdot \bar{\bar{\mu}}_r^{-1} \cdot (\nabla \times \mathbf{E}) \; &- \; k_0^2 \mathbf{T} \cdot \bar{\bar{\epsilon}}_r \cdot \mathbf{E}\} dV \\ &+ \iiint_{V_s} \mathbf{T} \cdot \left( jk_0 Z_0 \mathbf{J}^i + \nabla \times \bar{\bar{\mu}}_r^{-1} \cdot \mathbf{M}^i \right) dV \\ &+ jk_0 Z_0 \iint_{S_0+S_f} \mathbf{T} \cdot (\mathbf{H} \times \hat{n}) dS = 0 \end{aligned} \tag{1}$$

where $\mathbf{E}$ and $\mathbf{H}$ denote the electric and magnetic fields, $\bar{\bar{\epsilon}}_r$ and $\bar{\bar{\mu}}_r$ are the relative tensor permittivity and permeability of the cavity filling (possibly inhomogeneous), $S_0$ represents the non-metallic portions of the aperture and $S_f$ denotes the junction opening to the feeding

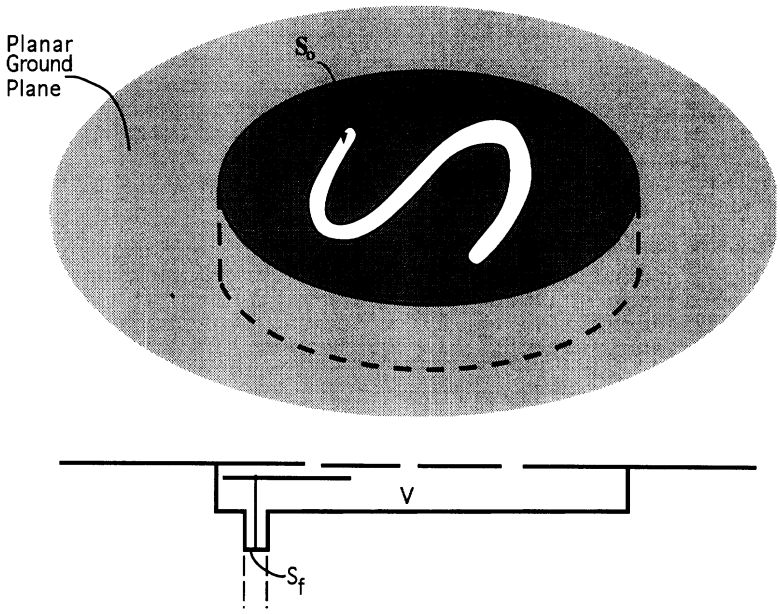


Figure 1: Geometry of a cavity-backed annular slot antenna in a ground plane

structures. As usual, $\mathbf{T}$ represents an appropriate testing/weighting function to be specified later. The volume $V_s$ refers to that occupied by the impressed sources $\mathbf{J}_i$ and $\mathbf{M}_i$. Also, note that the latter integral refers to $\mathbf{H}$ on the antenna aperture $S_o$ and the feed aperture $S_f$, typically located at the lower section of the cavity. Here, the unit normal $\hat{n}$ is directed outward from the boundary surfaces $S_o$ and $S_f$.

For a unique solution of (1) for $\mathbf{E}$ we require knowledge of $\mathbf{H}$ over $S_o$. In the context of the FE-BI method, the relation between $\mathbf{H}$ and $\mathbf{E}$ is determined by the boundary integral equation

$$\mathbf{H} = \mathbf{H}^{go} + 2jk_0Y_0 \iint_{S_0} (\hat{z} \times \mathbf{E}(\mathbf{r}'))G_0(\mathbf{r},\mathbf{r}')\, dS' + \frac{2jY_0}{k_0} \iint_{S_0} \nabla' \cdot (\hat{z} \times \mathbf{E}(\mathbf{r}'))\nabla G_0(\mathbf{r},\mathbf{r}')\, dS' \quad (2)$$

where

$$G_0 = \frac{e^{-jk_0R}}{4\pi R} \tag{3}$$

is the free space Green's function with $R = |\mathbf{r} - \mathbf{r}'|$. For this problem, $\mathbf{H}^{go}$ is equal to the sum of the incident and ground plane reflected fields for scattering and zero for antenna analysis.

To construct a linear set of equations from (1) and (2), we must first tessellate the volume and introduce expansions for each of the tessellation elements. We can choose, among a variety of standard volume tessellation elements, including bricks, tetrahedrals and prisms [12]. For printed antenna applications, the cavity depth is typically kept constant but the antenna shape (slot and printed configuration) can be of any arbitrary configuration. Examples include spiral antennas, log periodics, narrow slot elements, patches of various shapes as well as frequency selective surfaces employing resonant elements of various shapes. Thus, for this application, the chosen tessellation elements can be of constant depth but must be more adaptable for surface modeling. The edge-based prismatic elements presented in [11],[10],[JinFa Lee] allows for this type of flexibility while at the same time provide for meshing simplifications. In essence, for this application, prismatic elements, provide the advantage that once the surface mesh of the cavity (including the antenna elements) is constructed, the volume mesh can be generated by simply growing the mesh downwards within the interior of the cavity volume.

Choosing prisms as the tesselation elements (see Figure 2), the field is expanded within the cavity volume as

$$\mathbf{E}^e = \sum_{j=1}^{9} E_j^e \mathbf{W}_j^e = [\mathbf{W}]_e^T \{E^e\} \tag{4}$$

where $[\mathbf{W}]_e = [\{W_x\}, \{W_y\}, \{W_z\}]$ and $\{E^e\} = \{E_1^e, E_2^e, \ldots, E_9^e\}^T$ are specified explicitely

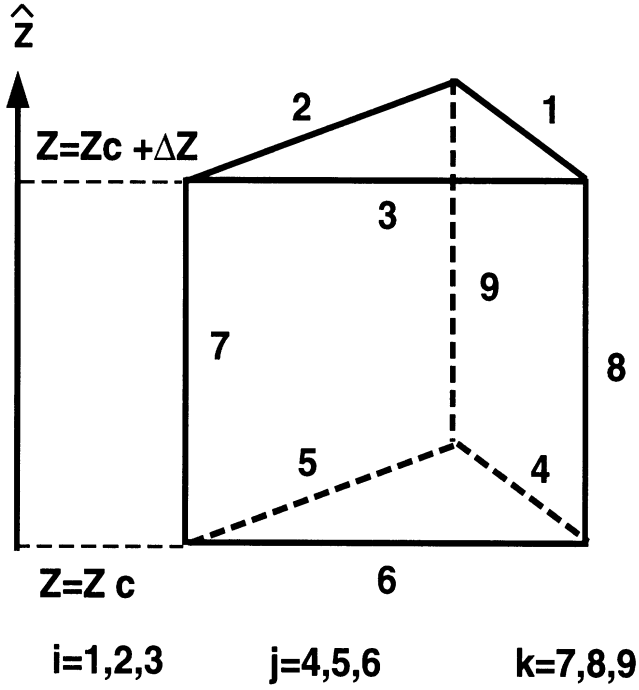


Figure 2: Right angled prism

in [10]. On the aperture, since the top and bottom faces of the prism are triangles, these reduce to

$$\mathbf{E}^s(\mathbf{r}) = \sum_{i=1}^{3} E_i^s \mathbf{S}_i^s(\mathbf{r}) = [S]_s^T \{E^s\} \tag{5}$$

where $[S]_s = [S_x, S_y]$ and

$$\mathbf{S}_i = \frac{l_i}{2A^e} \hat{z} \times (\mathbf{r} - \mathbf{r}_i) \tag{6}$$

Here, $\mathbf{r}$ and $\mathbf{r}_i$ refer to the position vector within the triangle and at the $i^{th}$ node of the triangular face. The parameters $l_i$ and $A^e$ denote the length of the ith edge of the triangle and its area, respectively. We also observe that apart from its vector direction, $\mathbf{S}_i$ is simply

the roof-top basis function used in the usual moment method implementations [13]. To generate a linear system for the solution of $E_j^e$, (4) and (5) are substituted into (1) and (2) and Galerkin's method (setting $\mathbf{T} = \mathbf{W}$) is employed to yield

$$\sum_{e=1}^{N_v}[A^e]\{E^e\} + \sum_{s=1}^{N_s}[B^s]\{E^s\} + \sum_{e=1}^{N_v}\{K^e\} + \sum_{s=1}^{N_s}\{L^s\} = 0 \tag{7}$$

in which $N_v$ and $N_s$ indicate the number of volume and surface/aperture elements, respectively. The matrix elements are given by

$$A_{ij}^e = \iiint_{V_e}\{(\nabla \times \mathbf{W}_i)\cdot\bar{\bar{\mu}}_r^{-1}\cdot(\nabla\times\mathbf{W}_j) - k_0^2\mathbf{W}_i\cdot\bar{\bar{\epsilon}}_r\cdot\mathbf{W}_j\}dV \tag{8}$$

$$K_e^i = \iiint_{V_e}\mathbf{W}_i\cdot\left[jk_0Z_0\mathbf{J}^i + \nabla\times\bar{\bar{\mu}}_r^{-1}\cdot\nabla\times\mathbf{M}^i\right]dV \tag{9}$$

$$\begin{aligned} B_{ij}^s &= -\iint_{S_s}\iint_{S_s'} 2k_0^2\mathbf{S}_i^s(\mathbf{r})\cdot\mathbf{S}_j^s(\mathbf{r}')G_0(\mathbf{r},\mathbf{r}')dSdS' \\ &+ 2\iint_{S_s}\iint_{S_s'}[\nabla\times\mathbf{S}_i^s(\mathbf{r})]_z[\nabla'\times\mathbf{S}_j^s(\mathbf{r}')]_zG_0(\mathbf{r},\mathbf{r}')dSdS' \end{aligned} \tag{10}$$

$$L_i^s = 2jk_0Z_0\iint_{S_s}S_i^s\cdot(\mathbf{H}^i\times\hat{z})dS \tag{11}$$

and the final system of equation is obtained by carrying out the sum or assembly of the element equations given in (7). Doing so, the resulting matrix system takes the general form

$$[\mathcal{A}]\begin{Bmatrix}\{E^V\}\\ \{E^S\}\end{Bmatrix} + \begin{bmatrix}[0] & [0]\\ [0] & [\mathcal{B}]\end{bmatrix}\begin{Bmatrix}\{E^V\}\\ \{E^S\}\end{Bmatrix} = \begin{Bmatrix}\{b^V\}\\ \{b^S\}\end{Bmatrix} \tag{12}$$

In this system, $\{E^V\}$ denotes the field unknowns within the volume enclosed by $S_o$ whereas $\{E^S\}$ represents the corresponding unknowns on the boundary $S_o$. The excitation column $\{b^V\}$ results from the assembly of $\{K^e\}$, and $\{b^S\}$ is associated with incident field excitations (for scattering).

# 3 Fast Integral Methods for Dense Matrix-Vector Product Calculations

Typically, the system (12) is solved using iterative solvers [14],[15] to take advantage of the sparsity of the matrix $[\mathcal{A}]$. Since $[\mathcal{A}]$ has only 9 to 30 non-zero entries per row, whereas the matrix order $N_V$ is in the thousands, the execution of the matrix-vector product is an $O(N_V)$ operation and this is a major characteristic and advantage of FEM. However, the boundary integral matrix which is generated from the second term of (7) is a dense matrix and requires $O({N_S}^2)$ operations, where $N_S$ denotes the number of aperture edges. Therefore, the greatest CPU time in the iterative solver is expended in calculating the matrix-vector product $[\mathcal{B}]E^S$. To speed up its calculation, k-space methods [16],[17],[18] were considered several years back to cast the matrix in Toeplitz form. In this case, a rectangular surface grid is employed but unfortunately these lead to approximations of the geometrical specification of the modeled structure.

This method was extended to handle triangular grids [9] by mapping them to rectangular ones using linear interpolations. Such interpolations were found of acceptable accuracy when the mapped grid was not highly distorted from the triangular. Also, the interpolation cannot

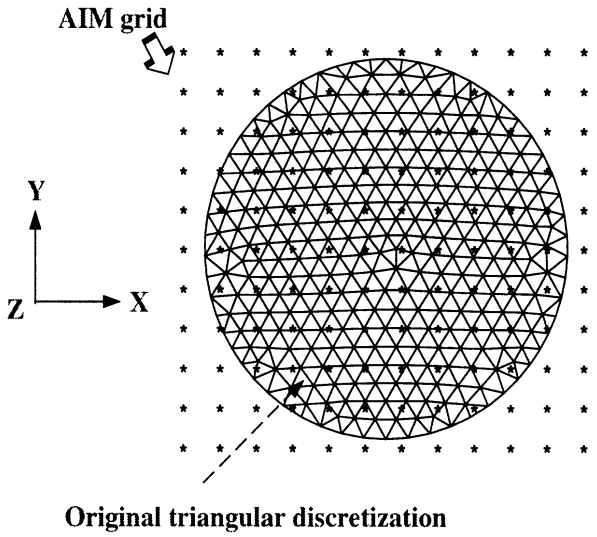


Figure 3: Mapping of the original triangular grid to a uniform AIM grid.

be employed with confidence in cases where the triangular grid contains very fine details as is the case with slot and printed antennas such as spirals, log-periodics, etc. unless excessively small uniform rectangular grids are also used. This is not, of course, highly undesirable since it leads to a substantial increase from the original degrees of freedom (DOFs) or unknowns.

More recently, the fast multipole method (FMM) [3],[4],[6] was employed in conjunction with the finite element method for speeding-up the calculation of the boundary integral matrix-vector product. FMM reduces the CPU requirements down to $O(N^{1.5})$ or even lower by using the multilevel FMM. However, this speed-up is realized for large computational domains and moreover FMM works on the original triangular grid. For antennas, the aperture grid may not be large in terms of wavelengths (unless dealing with arrays) but it may be highly dense resulting in excessively large DOFs. Thus FMM must still deal with the large boundary DOFs and for small apertures the speed-up benefits may not be realized.

An alternative fast integral method is the adaptive integral method(AIM) which was introduced by Bleszynski et. al. [1]. This approach is similar to the k-space method in several respects but is devoid of geometrical inaccuracies. Much like the approach in [9], AIM also introduces a coincident equi-spaced rectangular grid over the original unstructured triangular grid (see Figure 3). However, in the case of AIM, delta sources are placed at the nodes of the rectangular grid to represent the exterior radiated or scattered field by the cavity. The strength and polarization of these sources is found by enforcing equality of the moments between the original grid sources (edge fields) and the new delta sources on the rectangular grid. The following important observations make AIM attractive in computing the boundary integral matrix-vector product associated with the FE-BI system (12):

- The rectangular AIM grid can be chosen much coarser than the original antenna grid. Thus, small antenna details do not dictate the final DOFs used for calculating the final matrix-vector products.

- For antenna applications, there is little or no wastage of grid points which may lie beyond the aperture when the original grid is overlaid with the rectangular AIM grid. Thus, two dimensional FFTs can be efficiently employed for calculating the matrix-vector products as done in [17],[18].

- The near zone matrix elements are calculated using the original boundary matrix and discrete elements. Thus, as in the case of FMM (but not so with the implementation in [9] and [19]), AIM makes no compromises in modeling the near zone interactions. In the implementation of AIM, this is achieved by decomposing the matrix into two

submatrices, one containing the near zone interactions (a sparse matrix) and another representing the interactions of the equivalent sources on the AIM rectangular grid. The latter can be written as a product of sparse and Toeplitz.

- Using AIM, the CPU requirements for the boundary integral matrix-vector product is $O(N_S log N_S)$ for large $N_S$ and this is a consequence of the Toeplitz/Circulant nature of the boundary matrix associated with the uniform AIM grid.

# 4 Fast BI computation with AIM

As noted in the previous section, the purpose of AIM is to perform fast computation of the BI matrix-vector product $[\mathcal{B}]\{E^S\}$ in (12). The objective of AIM is to cast the system into a Toeplitz format. This is achieved by first splitting the matrix as

$$[\mathcal{B}] = [\mathcal{B}^{near}] + [\mathcal{B}^{far}] \tag{13}$$

based on a threshold distance referred to as the near-zone radius. The matrix $[\mathcal{B}^{near}]$ contains the interactions between elements separated less than the threshold distance, whereas $[\mathcal{B}^{far}]$ contains the remaining interactions. The elements of $[\mathcal{B}^{near}]$ are evaluated with the exact procedure while those of $[\mathcal{B}^{far}]$ and the product $[\mathcal{B}^{far}]\{E^S\}$ are evaluated in an approximate manner.

Application of AIM requires that the whole geometry be enclosed in a regular rectangular grid. Basically, the fields of each interior edge is re-expressed using a new expansion based on delta sources located at the nodes of the uniform AIM grid. For the $m^{th}$ edge, this new

expansion has the form

$$\overline{\psi}_m = \sum_{q=1}^{M^2} \delta(x - x_{mq})\delta(y - y_{mq})[\Lambda^x_{mq}\hat{x} + \Lambda^y_{mq}\hat{y}] \tag{14}$$

where $\mathbf{r}_{mq}$ are the position vectors of $M^2$ points on the square surrounding the center of the edge and $\delta(x)$ is the usual Dirac delta function. The coefficients $\Lambda^{x,y}_m$ are suitably chosen so that the new expansion is equivalent to the original representation using triangular elements. A similar expansion is used for the divergence of the basis functions

$$\psi^d_m = \sum_{q=1}^{M^2} \delta(x - x_{mq})\delta(y - y_{mq})\Lambda^d_{mq} \tag{15}$$

To find a relation between the $\Lambda^{x,y}_m$ and $I_n$ coefficients, we equate moments of the two expansions up to order M. Specifically, we set

$$\mathbf{M}^m_{q_1,q_2} = \mathbf{F}^m_{q_1,q_2} \tag{16}$$

where

$$\begin{aligned} \mathbf{M}^m_{q_1 q_2} &= \int_{-\infty}^{\infty}\int_{-\infty}^{\infty} \overline{\psi}_m (x - x_a)^{q_1}(y - y_a)^{q_2} dxdy \quad for \;\; 0 \le q_1, q_2 \le M \\ &= \sum_{q=1}^{M^2} (x_{mq} - x_a)^{q_1}(y_{mq} - y_a)^{q_2}[\Lambda^x_{mq}\hat{x} + \Lambda^y_{mq}\hat{y}] \;\; with \;\; q = q_1 + q_2 \end{aligned} \tag{17}$$

$$\mathbf{F}^m_{q_1 q_2} = \int_{-\infty}^{\infty}\int_{-\infty}^{\infty} \mathbf{S}_m (x - x_a)^{q_1}(y - y_a)^{q_2} dxdy \tag{18}$$

Similarly, by equating moments of $[\nabla \times \mathbf{S}]_z$ with the new expansion (15), we establish a relation between $\Lambda^d_m$ and $I_n$. That is, we set

$$D^m_{q1,q2} = H^m_{q1,q2} \tag{19}$$

where

$$D^m_{q_1 q_2} = \int_{-\infty}^{\infty}\int_{-\infty}^{\infty} \psi^d_m (x - x_a)^{q_1} (y - y_a)^{q_2} dx dy = \sum_{q=1}^{M^2} (x_{mq} - x_a)^{q_1} (y_{mq} - y_a)^{q_2} \Lambda^d_{mq} \tag{20}$$

$$H^m_{q_1 q_2} = \int_{-\infty}^{\infty}\int_{-\infty}^{\infty} [\nabla \times \mathbf{S}_m]_z (x - x_a)^{q_1} (y - y_a)^{q_2} dx dy \tag{21}$$

(16) and (19) give three $M^2 \times M^2$ systems yielding the equivalence coefficients as the solution.

Were we to use the equivalent expansions to represent the currents everywhere, the resulting impedance matrix will be of the form

$$[\mathcal{B}]^{total}_{AIM} = \sum_{i=1}^{3} [\Lambda]_i [G] [\Lambda]^T_i \tag{22}$$

In this, $[\Lambda]_i$ are the sparse matrices containing the coefficients of the expansion (14) and (15) whereas $[G]$ is the Toeplitz matrix whose elements are the free space Green's function evaluated at the grid points. It has been shown [1] that $[\mathcal{B}]^{total}_{AIM}$ is not of sufficient accuracy for modeling the interactions between the nearby current elements. To take advantage of the Toeplitz structure of $[G]$ and sparsity of $[\Lambda]$ we can still use $[\mathcal{B}]^{total}_{AIM}$ to represent the far element interactions. However, we will retain the exact interaction matrix elements for the near element interactions. That is, we rewrite $[\mathcal{B}]^{total}_{AIM}$ as

$$[\mathcal{B}]^{total}_{AIM} = [\mathcal{B}]^{near}_{AIM} + [\mathcal{B}]^{far}_{AIM} \tag{23}$$

Comparing this to (13) and setting $[\mathcal{B}]^{far} \simeq [\mathcal{B}]^{far}_{AIM}$ we can rewrite the original $[\mathcal{B}]$ matrix as

$$[\mathcal{B}] \simeq ([\mathcal{B}]^{near} - [\mathcal{B}]^{near}_{AIM}) + [\mathcal{B}]^{total}_{AIM} \tag{24}$$

or

$$[\mathcal{B}] \simeq [S] + \sum_{i=1}^{3} [\Lambda]_i [G] [\Lambda]^T_i \tag{25}$$

where $[S] = [\mathcal{B}]^{near} - [\mathcal{B}]^{near}_{AIM}$ is a sparse matrix corresponding to the difference between the near field interactions computed by the standard boundary integral technique and AIM. The Toeplitz property of the Green's function, defined on the regular grid, enables use of the FFT to accelerate the computation of the matrix-vector product. The sequence of operations involved in the construction of the coefficient and Green's function matrices are indicated in Figure 4(a); those for the matrix-vector product execution are outlined in Figure 4(b). In the computation of the matrix-vector product, the initial step of transforming the currents from the original MM grid onto the uniform AIM grid is comparable to the grouping operation of the FMM. While the FMM relies on grouping to reduce the number of scattering centers, the sequence of operations in AIM can be interpreted as a realignment of scattering centers onto a regular grid. Although, this process does not reduce the number of scattering centers, the regularity of their location enables use of the FFT for fast computation of matrix-vector products.

# 5 Results

A computer code based on the discussed formulation was implemented. The first step was to validate the spatial-domain FE-AIM formulation with results from a spectral domain FE-BI formulation. Figure 5 compares the spatial domain FE-AIM solution with a spectral-domain FE-BI solution presented in [20] for the scattering by a cavity-backed patch antenna. Having accomplised such a validation, the results presented in Figures 6-10 compare spatial domain FE-BI and FE-AIM solutions, to demonstrate the savings in memory and CPU time. Figure 6 shows the radiation pattern for an annular slot computed in the elevation plane, $\phi = 5^0$.

The reference FE-BI solution [10] is contrasted with computations of BI using AIM (indicated as FE-AIM). It is seen that for this example, the threshold distance in AIM can be reduced to $0.25\lambda$ without significant loss of accuracy. This enables the reduction of matrix entries stored in the near field portion by a factor of three resulting in a corresponding savings in memory as indicated in the tabulation of the near-zone non-zero entries. Figure 7 shows the radiation pattern for the same antenna in the $\phi = 90^0$ elevation plane. The normal direction in this plane, reveals the characteristic separation between co-polarization and cross-polarization levels for the annular slot at observation angles close to normal in the elevation plane. From this figure, it is gleaned that the threshold distance in AIM can be reduced down to even $0.15\lambda$ if an average error of a dB could be tolerated. From the computation of near-zone matrix entries, such a threshold would result in a factor of five saving in memory. Figure 8 shows a scattering cross-section for the same slot but at a frequency of 0.73 GHz (at which the antenna is electrically even smaller) instead of the previous 1 GHz. It should be noted that for a threshold of $0.4\lambda$ (larger than the diameter of the BI contour) the near-zone and far-zone entries for AIM cancel each other in accordance with (24), thus yielding a very small error (0.00086 dB) in comparison to the FE-BI solution. A quantity of vital importance in antenna computations is input impedance. Figure 9 depicts the input impedance of a very narrow probe-fed annular slot, computed using FE-BI and FE-AIM. The probe is placed at $y = 0$. It is seen that evaluation of the boundary integral with AIM enables the reduction of the near-zone non-zeros by more than half. Computation of input impedance demands very high accuracy and the threshold distance was held constant at 10.5 cm (corresponding to $0.35\lambda$ at 1 GHz and $0.49\lambda$ at 1.4 GHz - the corresponding diameter of the entire BI contour

varying from $0.513\lambda$ to $0.718\lambda$). While, Figures 6-9 demonstrate the ability of AIM to translate very fine details such as a narrow slot onto a coarser equivalent grid, Figure 10 and 11 indicate the importance of a low threshold distance in modeling cavity-backed antenna arrays. Figure 10 and 11 indicate that for an average error of less than a dB in scattering and radiation patterns it is possible to reduce the number of non-zeros in the near-zone part of the impedance matrix by a factor of six, resulting in substantial saving in memory. This is a consequence of employing a threshold distance of 10 cm, which is about a fifth of the cavity diameter. It is necessary to note that employing such a threshold distance results in a majority of the interactions between different slots being treated with the AIM procedure. This is of paramount importance in modeling antenna arrays and spiral antennas.

## 5.1 Summary

AIM, with its low threshold distance, and ability to translate to an equivalent grid is capable of saving a significant amount of memory and solution time for bodies which are finely discretized even though they may not be electrically large. Its accuracy is preserved even while performing radiation computations thus making it the method of choice for analyzing antennas with intricate details.

# References

[1] E. Bleszynski, M. Bleszynski, and T. Jaroszewicz, "AIM: Adaptive integral method for solving large-scale electromagnetic scattering and radiation problems," *Radio Science*,

vol. 31, no. 5, pp. 1225–1251, 1996.

[2] V. Rokhlin, "Rapid solution of integral equations of scattering theory in two dimensions," *Journal of Computational Physics*, vol. 86, no. 2, pp. 414–439, 1990.

[3] S.S. Bindiganavale and J.L. Volakis, "Comparison of three FMM techniques for solving hybrid FE-BI systems," *IEEE Antennas and Propagation Magazine*, vol. 39, pp. 47–59, August 1997.

[4] S. S. Bindiganavale and J. L. Volakis, "A hybrid FEM-FMM technique for electromagnetic scattering," *IEEE Transactions on Antennas and Propagation*, vol. 45, no. 1, pp. 180–181, 1997.

[5] S. S. Bindiganavale and J. L. Volakis, "Comparison of fast integral mesh truncation schemes for hybrid FE-BI systems," *IEE Electronics Letters*, vol. 33, no. 11, pp. 924–925, 1997.

[6] N. Lu and J. M. Jin, "Application of the fast multipole method to finite element-boundary integral solution of scattering problems," *IEEE Transactions on Antennas and Propagation*, vol. 44, no. 6, pp. 781–786, 1996.

[7] J.M. Jin and J.L. Volakis, "A hybrid finite element method for scattering and radiation by microstrip patch antennas and arrays residing in a cavity," *IEEE Transactions on Antennas and Propagation*, vol. 39, pp. 1598–1604, November 1991.

[8] J.L. Volakis, T. Özdemir, and J.Gong, "Hybrid finite element methodologies for antennas and scattering," *IEEE Transactions on Antennas and Propagation*, vol. 45, pp. 493–507, March 1997.

[9] J. Gong, J.L. Volakis, and A.C. Woo, "A hybrid finite element-boundary integral method for the analysis of cavity-backed antennas of arbitrary shape," *IEEE Transactions on Antennas and Propagation*, vol. 42, no. 9, pp. 1233–1242, 1994.

[10] J. Gong, J.L. Volakis, and H.T.G. Wang, "Efficient finite element simulation of slot antennas using prismatic elements," *Radio Science*, vol. 31, no. 6, pp. 1837–1844, 1996.

[11] T. Özdemir and J.L. Volakis, "Triangular prisms for edge-based vector finite element analysis of conformal antennas," *IEEE Transactions on Antennas and Propagation*, vol. 45, pp. 788–797, May 1997.

[12] O.C. Zienkiewicz and R.L. Taylor, *The Finite Element Method.* McGraw-Hill: New York, 1989.

[13] S. Rao, D. Wilton, and A. Glisson, "Electromagnetic scattering by surfaces of arbitrary shape," *IEEE Transactions on Antennas and Propagation*, vol. 30, no. 3, pp. 409–418, 1982.

[14] Y. Saad, *Iterative methods for sparse linear systems.* PWS Publishing Company: Boston, 1996.

[15] J. L. Volakis, "Iterative solvers," *IEEE Antennas and Propagation Magazine*, vol. 37, pp. 94–96, December 1995.

[16] N.N.Bojarski, "k-space formulation of the electromagnetic scattering problem," Tech. Rep. AFAL-TR-71-5, USAF, March 1971.

[17] T.K. Sarkar, E. Arvas, and S.M. Rao, "Application of FFT and the conjugate gradient method for the solution of electromagnetic radiation from electrically large and small conducting bodies," *IEEE Transactions on Antennas and Propagation*, vol. 34, no. 5, 1986.

[18] J. L. Volakis and K. Barkeshli, "Applications of the conjugate gradient FFT method to radiation and scattering," in *Application of the Conjugate Gradient Method to Electromagnetics and Signal Analysis* (T. K. Sarkar, ed.), ch. 6, New York: Elsevier, 1991.

[19] C.Y.Shen, K.J.Glover, M.I.Sancer, and A.D.Varvatsis, "The discrete Fourier transform method of solving differential integral equations in scattering theory," *IEEE Transactions on Antennas and Propagation*, vol. 37, pp. 1032–1049, August 1989.

[20] A.C. Polycarpou, M.R. Lyons, J. Aberle, and C.A. Balanis, "Analysis of arbitrary shaped cavity-backed patch antennas using a hybritization of the finite element and spectral domain methods," in *1996 IEEE Int. Symp. on Antennas and Propagation Digest*, July 1996.

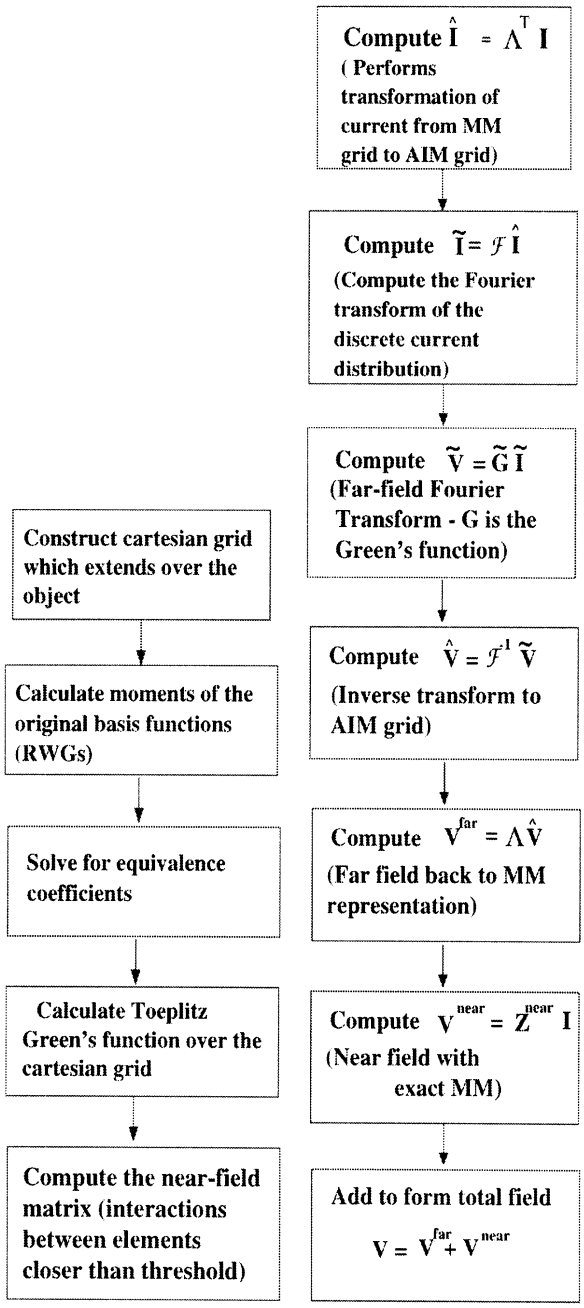


Figure 4: (a) Matrix build operations and (b) Matrix vector product computation in AIM

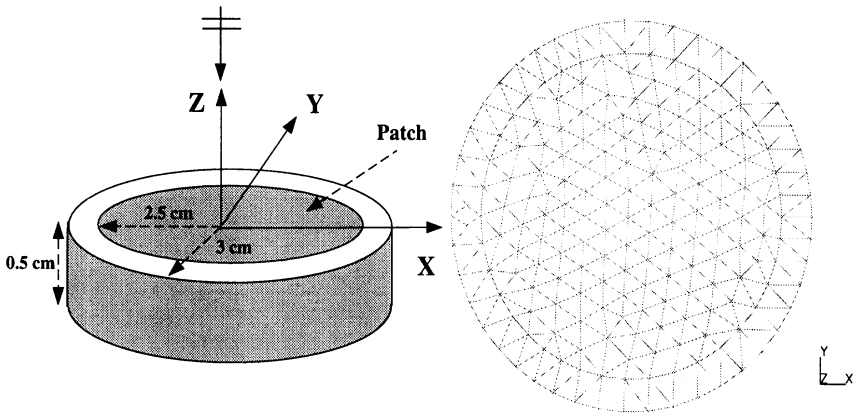


(a)

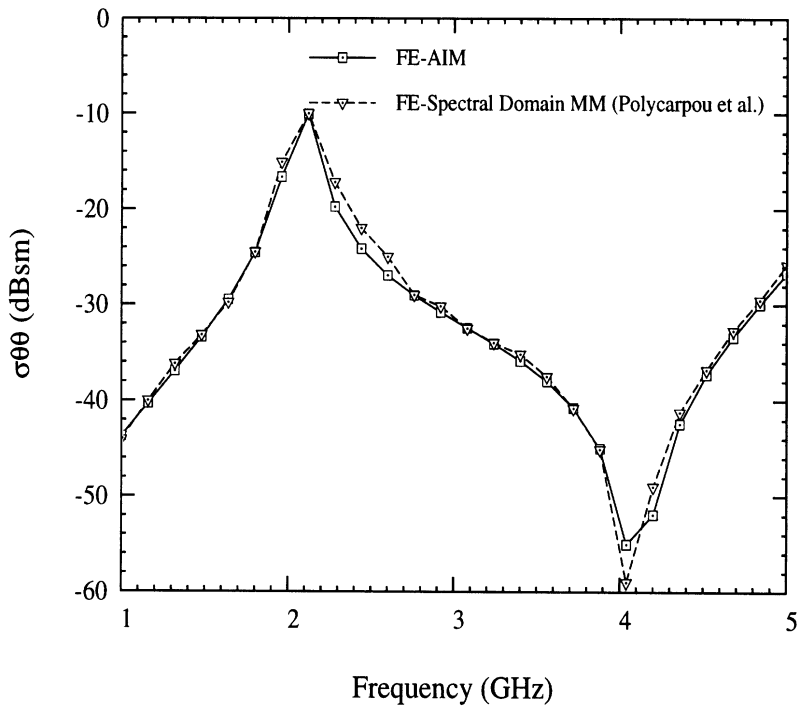


(b)

Figure 5: (a) Geometry and surface discretization of a cavity-backed patch antenna (b) Monostatic RCS at normal incidence versus frequency - cavity filling has a $\epsilon_r = 2.2 - j0.002$ and $\mu_r = 1$

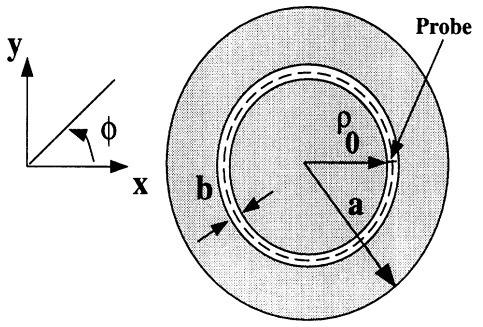


a = 12.35 cm
b = 0.75 cm
$\rho_0$ = 7.7 cm
Frequency = 1 GHz

| | Non-zeros in near Z matrix |
|---|---|
| FE-BI | 4656 |
| FE-AIM (0.53 λ) | 4656 |
| FE-AIM (0.35 λ) | 2245 |
| FE-AIM (0.25 λ) | 1537 |

| | Average Error (dB) | |
|---|---|---|
| | Co-pol | X-pol |
| FE-AIM (0.35 λ) | 0.4402 | 0.2998 |
| FE-AIM (0.25 λ) | 0.6343 | 0.5334 |

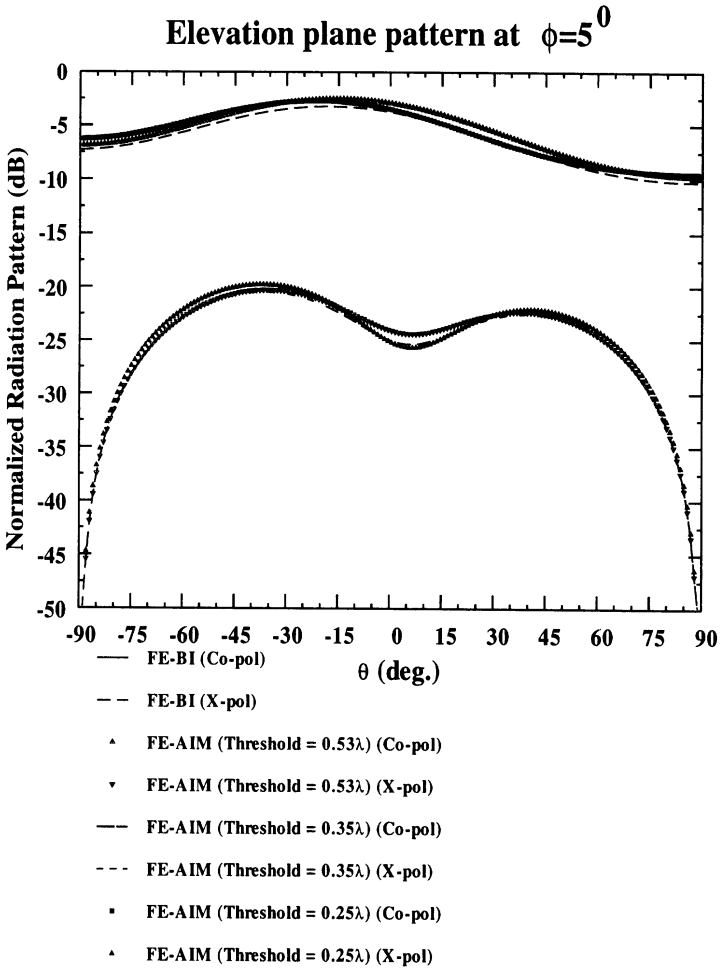


Figure 6: Radiation pattern from an annular slot in the $\phi = 0^0$ elevation plane

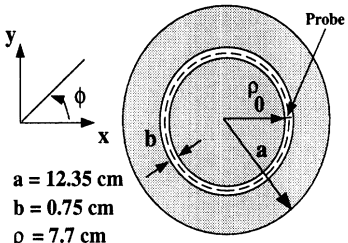


a = 12.35 cm
b = 0.75 cm
$\rho_0$ = 7.7 cm
Frequency = 1 GHz

| | Non-zeros in near Z matrix |
|---|---|
| FE-BI | 4656 |
| FE-AIM (0.15 λ) | 915 |
| FE-AIM (0.25 λ) | 1537 |
| FE-AIM (0.35 λ) | 2245 |

| | Average Error (dB) | |
|---|---|---|
| | Co-pol | X-pol |
| FE-AIM (0.15 λ) | 1.0524 | 1.0373 |
| FE-AIM (0.25 λ) | 0.6142 | 0.9105 |
| FE-AIM (0.35 λ) | 0.876 | 0.2506 |

(a)

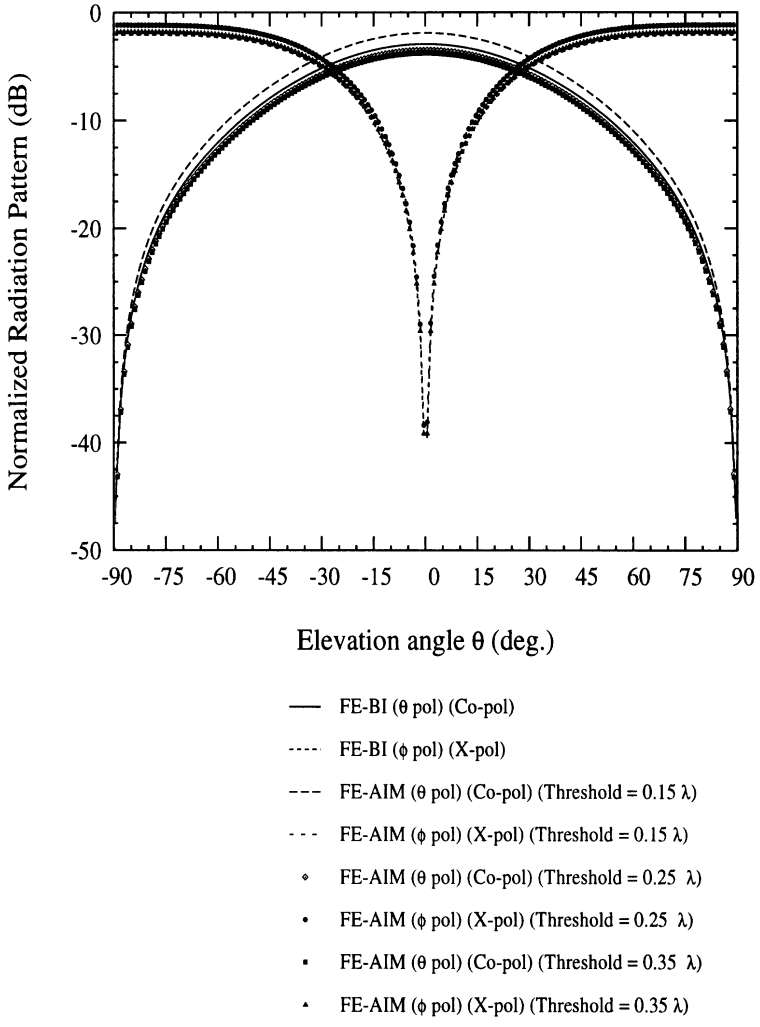


(b)



Figure 7: Radiation pattern from an annular slot in the $\phi = 90^0$ elevation plane

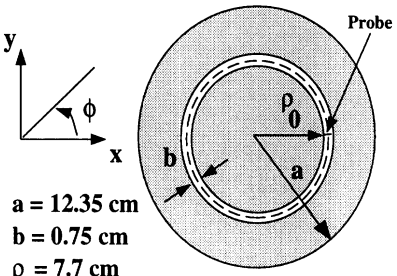


a = 12.35 cm
b = 0.75 cm
$\rho_0$ = 7.7 cm
Frequency = 0.73 GHz

| | Non-zeros in near Z matrix | Average Error (dB) Co-pol |
|---|---|---|
| FE-BI | 4656 | |
| FE-AIM (0.25 λ) | 2184 | FE-AIM (0.25 λ) 1.3124 |
| FE-AIM (0.33 λ) | 3272 | FE-AIM (0.33 λ) 1.0666 |
| FE-AIM (0.4 λ) | 4656 | FE-AIM (0.4 λ) 0.00086 |

(a)

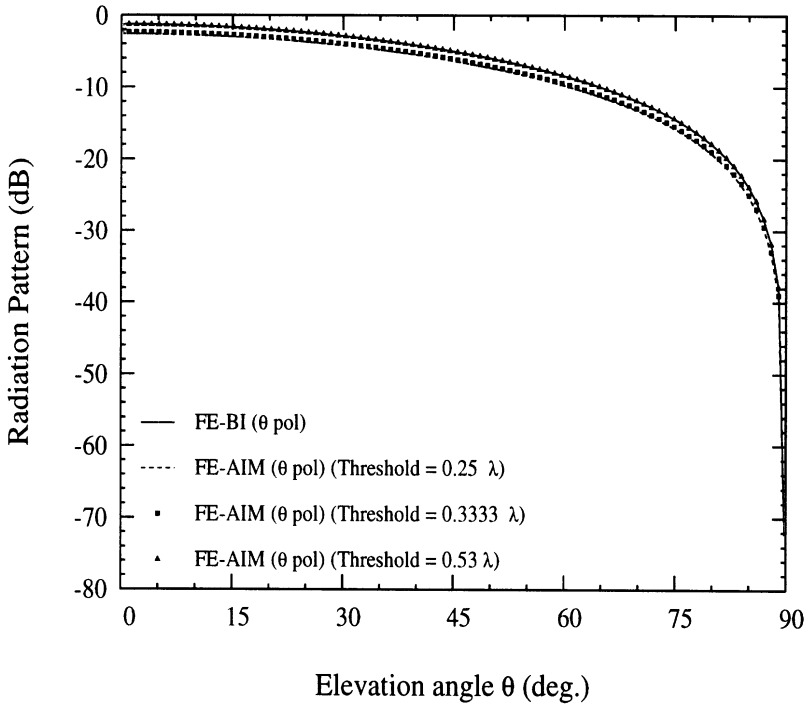


(b)

Figure 8: Bistatic scattering pattern from an annular slot; Normal incidence in the $\phi = 0^0$ plane and observation is in the $\phi = 90^0$ elevation plane

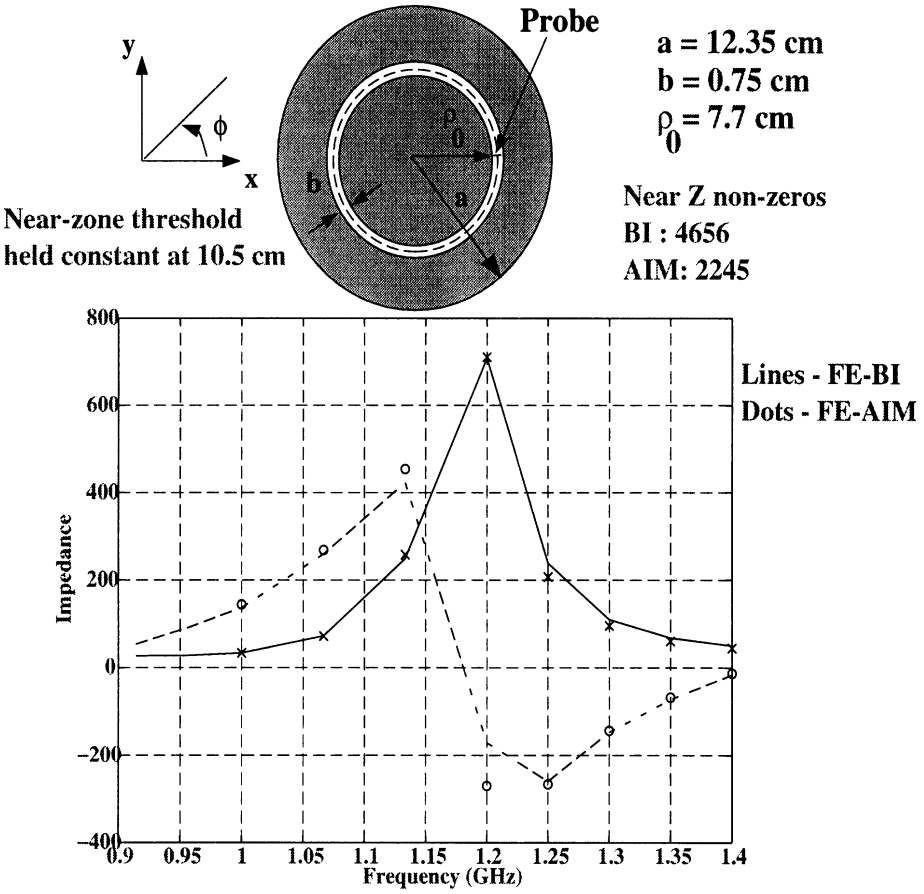


| Frequency (GHz) | FE-BI | FE-AIM |
|---|---|---|
| 1.0667 | 71.74 + j259.04 | 71.46 + j268.51 |
| 1.1333 | 248.51+j422.88 | 258.03 + j453.73 |
| 1.2 | 708.59-j170.31 | 710.39 - j269.71 |
| 1.25 | 238.47-j259.27 | 206.96 - j266.05 |
| 1.3 | 109.77-j146.96 | 95.48 - j142.82 |
| 1.35 | 67.63 - j71.61 | 59.84 - j 67.16 |
| 1.4 | 49.7 - j16.48 | 44.42-j12.95 |

Figure 9: Input impedance of a very narrow annular slot computed with FE-BI and FE-AIM

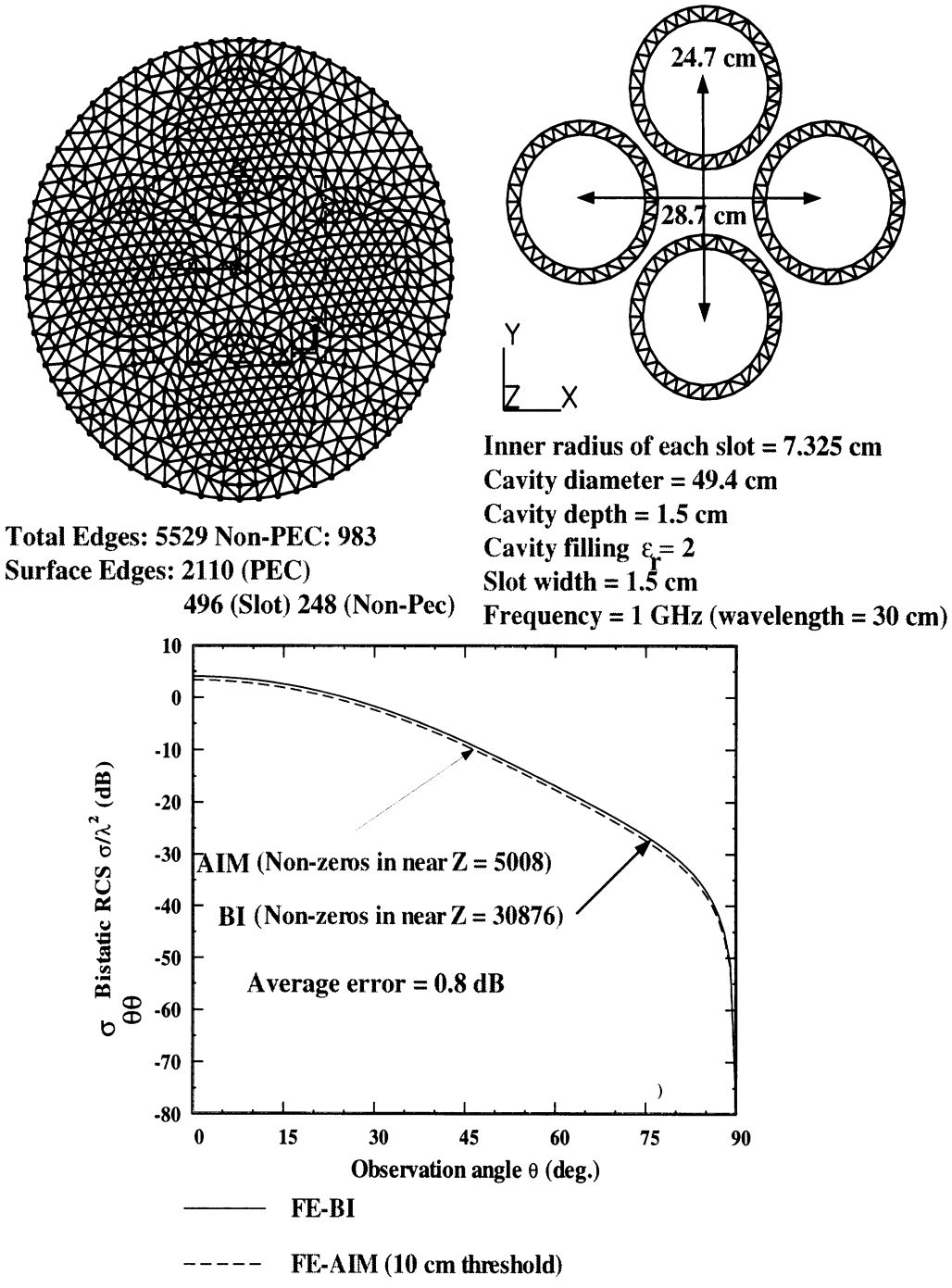


Figure 10: Bistatic RCS at normal incidence ($\phi = 90^0$ plane) from a cavity-backed slot array computed with FE-BI and FE-AIM

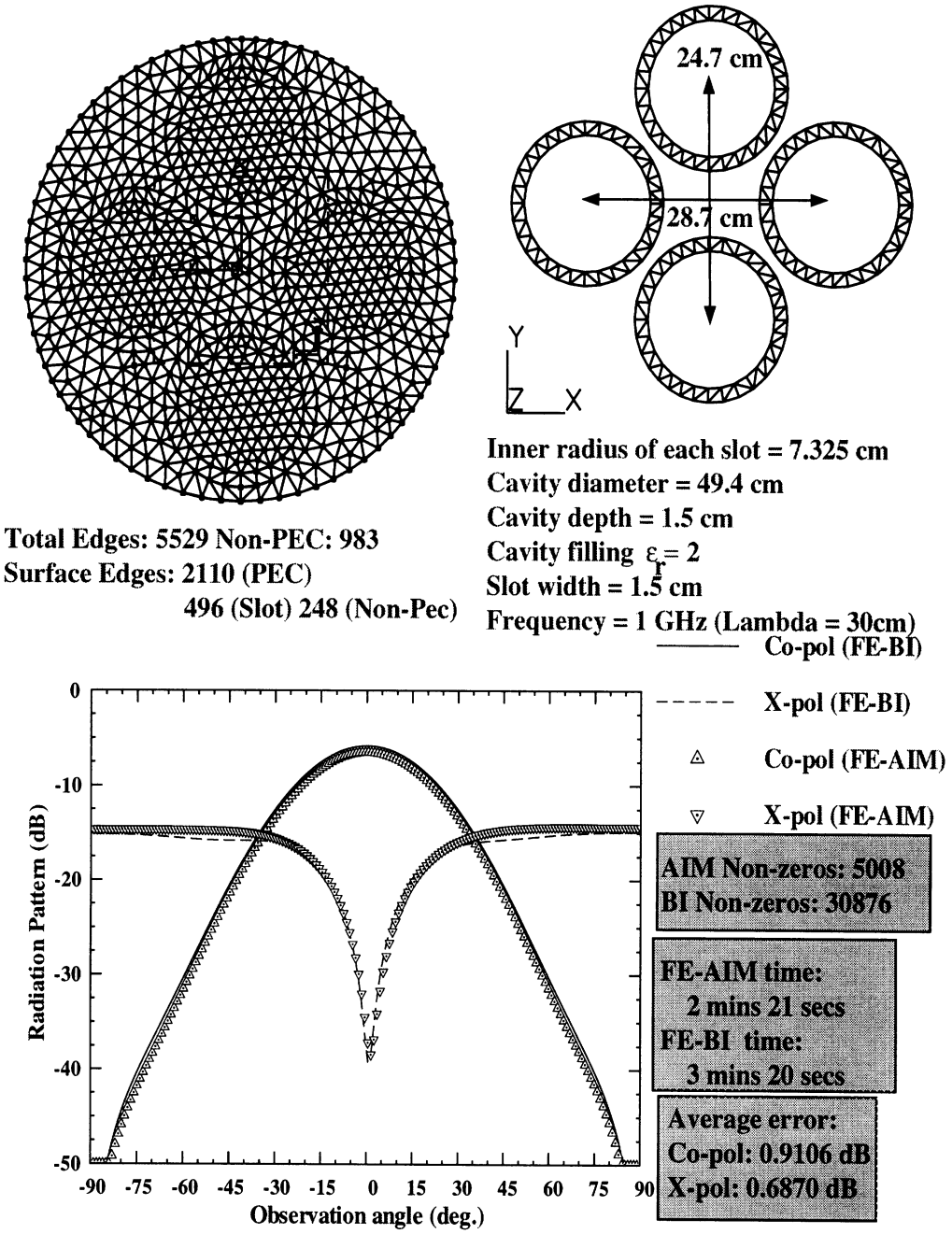


Figure 11: Radiation from a cavity-backed slot array computed with FE-BI and FE-AIM in the $\phi = 90^0$ plane